Pergamon

Prog. Energy Combust. Sci. Vol. 23, pp. 283–301, 1997

0360–1285/97 $29.00

PII: S0360-1285(97)00009-9

SOOT IN COAL COMBUSTION SYSTEMS*

Thomas H. Fletcher[†‡], Jinliang Ma[†], James R. Rigby[§], Alexander L. Brown[§] and Brent W. Webb[§]

[†]*Chemical Engineering Department, Brigham Young University, Provo, UT 84602, U.S.A.*
[§]*Mechanical Engineering Department, Brigham Young University, Provo, UT 84602, U.S.A.*

Abstract—Soot is generated from coal when volatile matter, tar in particular, undergoes secondary reactions at high temperatures. A description of soot in coal flames allows better calculations of radiative transfer and temperatures in near-burner regions, which in turn allows more accurate predictions of NO_x formation in coal-fired furnaces. Experiments are reviewed that examine the formation, agglomeration and properties of coal-derived soot, including pyrolysis experiments and combustion experiments. This review includes the types of experiments performed, the soot yields obtained, the size of the soot particles and agglomerates, the optical properties of soot, the relationship between coal-derived soot and soot from simple hydrocarbons, and attempts to model soot in coal flames. © 1997 Elsevier Science Ltd.

Keywords: coal, pyrolysis, soot.

CONTENTS

NOMENCLATURE

Symbol	Definition
c	constant (Eq. (1))
C_λ	absorption constant, spectral absorption index
CS	cross-section
e	charge on an electron
f_v	soot volume fraction
g	dispersion constant
i	imaginary component
I	intensity
k	complex component of index of refraction
L	path length
m	complex index refraction, mass
n	real component of index of refraction
N	number density of electrons
Q_e	extinction efficiency
T	temperature
α_λ	fitting coefficient (Eq. (1))
ϵ	complex dielectric function, emissivity
ϵ_o	dielectric constant
κ_λ	absorption coefficient
β_λ	extinction coefficient
λ	wavelength
τ	transmittance
ω	dispersion constant
Subscripts	
a	absorption
b	bound electron
e	extinction
f	free electron
p	plasma frequency
s	scattering
λ	wavelength
o	initial

* This paper was written as part of a series of review papers resulting from the 10th Annual Meeting of the Advanced Combustion Engineering Research Center (ACERC), held at the University of Utah in April 1996.

‡ Corresponding author.

1. INTRODUCTION

Small submicron carbonaceous particles, known as soot, are commonly observed in the combustion and pyrolysis of hydrocarbons. Soot is formed in many practical combustion systems ranging from a burning candle to sophisticated combustors such as gas turbines and internal combustion engines. Based on the experiments conducted on simple hydrocarbon flames, such as diffusion and premixed flames, it is found that soot is usually formed when conditions are sufficiently fuel rich to allow condensation or polymerization reactions of the fuel (and its initial decomposition products) to compete with oxidation[1]. Soot in those hydrocarbon flames usually exists in the form of both individual particles and agglomerates comprised of between several and thousands of primary particles.

Soot formation has also been observed in many coal utilization processes, including coal gasification and combustion. In a conventional wall-fired, swirl-stabilized, pulverized coal combustor, coal particles with mass mean diameters of approximately 50 μm are transported by primary air, and are injected into the furnace through the nozzles of a pulverized coal burner. When low NO_x burners are used along with staged combustion configuration, the region near the burner is fuel rich; the particles are rapidly heated at 10^4 to 10^6 K s^{-1} by convection from the recirculating hot gases and by radiation from the combustor walls and hot flame in the combustor. Many chemical and transport processes occur in a coal flame. Pyrolysis is the initial reaction step that occurs in a coal particle. Primary pyrolysis products include light gases, char, and tar, which is a mixture of heavy-molecular-weight hydrocarbons that exist as a gas at high temperatures and that condenses at room temperature. In the presence of oxygen, primary pyrolysis products are oxidized to form CO, CO_2, and H_2O (as well as several minor products). The volatile matter released in the gas phase may also undergo secondary reactions due to the high temperatures present in many combustors. Soot is one of the products of these secondary reactions. The tar from primary pyrolysis consists of many polycyclic aromatic hydrocarbons (PAH). These hydrocarbon molecules are very likely to undergo both cracking and polymerization processes at high temperature. Coal and coal tar contain a significant number of heteroatoms, consisting mainly of oxygen atoms but with some sulfur and nitrogen atoms as well. Estimated molecular weight distributions of coal tar range from 200 to 1000 Da. These tar molecules are therefore much larger and more chemically diverse than the simple hydrocarbon fuels generally used for studies of soot formation.

Soot in coal flames is important to combustion systems in part because of its radiative heat transfer effects. On a mass basis, there is much less soot present in a coal flame than other solid particles such as char and ash. However, the small size of soot particles results in a large total surface area. The importance of coal-derived soot in radiative heat transfer has been addressed by several researchers[2–4]. In a computational study of radiative heat transfer in a 915-MW coal-fired furnace by Ahluwalia and Im[4,5], where 10% of the volatile matter was assumed to be transformed into soot, it was found that the soot particles significantly enhanced radiative heat transfer. In spite of the fact that soot particles are only present in the flame zone, the calculated total radiative heat transfer was about 10% higher if soot was included in addition to gas, char and ash. This increase in heat transfer corresponded to an 80 K difference in predicted exit gas temperature. It can be expected that in the presence of a large radiant surface area of soot, the near-burner flame temperature could be lowered several hundred degrees due to the heat transfer to the surrounding walls[6].

A major problem in pulverized coal combustion is the formation of nitrogen oxides (NO_x) which are mainly generated (a) through the reaction of nitrogen and oxygen in air at elevated temperatures (called thermal NO_x), and (b) from the nitrogen-containing species or groups in the fuel (called fuel NO_x). It has been found that the production of both thermal and fuel NO_x in coal combustion is a strong function of reaction temperature. Therefore, the existence of soot in a coal flame will affect NO_x formation. Also, it has been reported that soot from coal pyrolysis contains nitrogen[7], and therefore soot is an additional pathway for fuel nitrogen evolution.

This review is divided into six parts: (a) types of experiments performed; (b) data from coal pyrolysis and combustion experiments; (c) nitrogen in coal-derived soot; (d) soot particle size; (e) optical properties of soot; and (f) modeling of soot formation and oxidation.

2. TYPES OF EXPERIMENTS PERFORMED

Several types of experiments have been performed to examine secondary reactions and soot formation from coal. These include: fixed bed pyrolysis followed by secondary reaction of volatiles; entrained flow pyrolysis experiments in inert gas; entrained flow combustion experiments; and entrained flow experiments in post-combustion gases. Since the type of experiment is coupled to the results obtained, the types of experiments are described in this section,

2.1. *Fixed-bed Pyrolysis Followed by Secondary Reaction*

Serio *et al.*[8] investigated kinetics of secondary reactions of fresh coal tars. The experiment consisted of two tubular reactors connected in series. The primary tar was generated in the first reactor by heating a helium-swept, shallow packed bed of a bituminous coal from room temperature to 550°C at a heating rate of 3 K min^{-1}. It was found that secondary reactions were insignificant for these conditions. The primary tar was then introduced to the secondary reactor, maintained at a

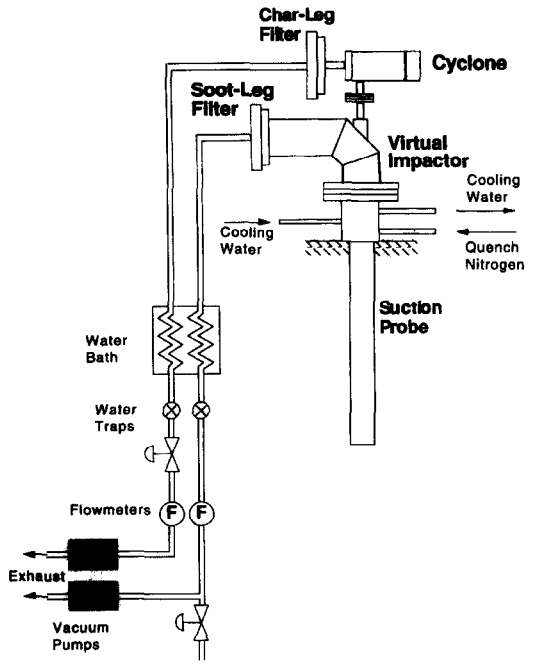

Fig. 1. Representative soot particle collection and separation system (adapted from Ma[6]).

constant temperature between 500 and 900°C, where decomposition reactions occurred. Extensive tar conversion (30–50%) was observed at 700–800°C, with light gases as the major products.

2.2. *Entrained Flow Pyrolysis Experiments in Inert Gas*

Entrained flow pyrolysis experiments in inert gas (argon or nitrogen) have been performed in drop tube reactors to determine the extent of secondary pyrolysis and soot formation as a function of temperature and residence time. This generally involves injecting cold particles into a hot gas, so that particle heating rates are high ($\sim 10^4$ K s^{-1}) to somewhat represent industrial conditions (10^5–10^6 K s^{-1}). Water-cooled collection probes use cold gas injection in the probe tip to achieve rapid particle cooling. After quenching, three types of particles are present in the gas stream in the probe: char particles, soot particles, and condensed tar particles. These must be separated in order to examine yields and properties of soot, char, and tar. The most common separation technique is aerodynamic separation, achieved by a virtual impactor and/or cyclone, with cutpoint diameters of 5 μm (i.e., the separation is designed such that 50% of the 5-μm particles are collected in each leg of the separation system)[7,9–13]. The most recent experiments have included a porous inner wall in the collection probe, through which quench gas transpires to minimize deposition of tar or soot inside the probe[7,12,13]. A representative collection system is shown in Fig. 1.

The tar and soot particles are collected on either glass fiber filters[7,9,11], used because of low pressure drop characteristics, or polycarbonate filters[12,13], used because samples can be scraped from the filter without contamination of glass fibers. The tar and soot are separated by dissolving the sample (on the glass fiber filter) in a suitable solvent such as dichloromethane or pyridine. The amount of tar/soot sample that does not dissolve is referred to as soot, while the amount that dissolves is referred to as tar. Obviously, questions arise as to the solubility of tar in the solvent used, and systems that avoid solvents are preferred.

Several variations of drop tube and collection systems have been used. The common drop tube experiments consist of injecting cold particles into a hot gas stream. In order to better control the extent of secondary reaction in the gas phase, while maintaining high enough coal particle temperatures to achieve significant devolatilization, some drop tubes have been operated in the radiant wall mode[7,14]. In the radiant wall mode, the main gas in the drop tube is relatively cold (< 700 K), but the walls are generally much hotter (1500–1800 K). The coal particles are generally small enough to be heated by radiation from the hot walls before the gas temperature rises due to convective heat transfer between the hot walls and the gas. In this mode of operation, the hot particles transfer heat by convection to the surrounding gas near the particle stream, and hence the local gas temperature can be somewhat controlled by the particle loading.

2.3. *Entrained Flow Combustion Experiments*

Single-particle combustion experiments have been performed in the post-flame gases of a flat flame burner, using a $CH_4/H_2/O_2/N_2$ flame to provide heat[15,16]. Coal particles were injected along the centerline of the reactor at feed rates low enough to achieve single-particle behavior. The equivalence ratio of the flame was adjusted to achieve the desired post-flame oxygen concentration. In these experiments, envelope flames developed around the individual particles due to the reaction of the volatiles released during pyrolysis with the surrounding oxygen. Soot formation in one experiment was observed optically by backlighting the particles, imaging the particles through a system of lenses and recording the images with high-speed cinematography[15]. In a similar experiment, holography was used to visualize the soot formed in the envelope flames around single particles[16].

2.4. *Entrained Flow Experiments in Post-combustion Gases*

Recent pyrolysis experiments have been performed with entrained coal particles in the post-flame gases of a $CH_4/H_2/N_2/O_2$ flat flame burner. These experiments were similar to the experiments performed by McLean *et al.*[15], but were conducted at high enough equivalence ratios to assure no O_2 in the post-flame gases. Therefore, the $CH_4/H_2/N_2/O_2$ provided both heat for the pyrolysis reactions and post-combustion gases (CO_2, H_2O, CO,

OH, etc.); this experiment may therefore be more representative of the fuel-rich region in a coal flame than experiments conducted in inert gases such as nitrogen or argon. These experiments were conducted at high temperatures (peak measured centerline gas temperatures of 1650, 1800, and 1900 K), and used both thermophoretic sampling[17] and bulk sampling using a suction probe, virtual impactor, and cyclone system as described above[6,13].

3. SOOT DATA FROM COAL PYROLYSIS AND COMBUSTION EXPERIMENTS

Volatiles released during primary coal pyrolysis contain PAH, which are susceptible to secondary pyrolysis reactions to form soot. Secondary reactions are complex, being influenced by coal type, heating rate, residence time, temperature, intra- and extraparticle heat and mass transfer, as well as by the physical structure of the reacting coal such as porosity, swelling, and softening characteristics[8]. Most of the studies on secondary coal pyrolysis chemistry have been conducted in inert environments.

3.1. *Model Compounds*

Several investigators have examined the pyrolysis of model compounds that are representative of coal tar. Wornat *et al.*[18] examined anthracene as a model coal-derived aromatic compound. Bruinsma *et al.*[19,20] studied the pyrolysis of many aromatic compounds using a coiled tube flow reactor. They found that benzene and its derivatives start to decompose in a temperature range from 800 to 1100 K. The thermal stability of benzene derivatives was found to increase in the following sequence: methoxy < thio < propyl < ethyl < carbaldehyde < ethenyl < hydroxyl < methyl < phenyl ≈ cyano < benzene. For heterocyclic compounds, thermal stability followed the sequence: furan < cyclopentadiene < pyrrole < pyridine < benzene < thiophene. In general, the longer attachments to aromatic compounds (such as propyl groups) are more likely to decompose at lower temperatures than short attachments (such as methyl groups). Also, 6-membered rings with no heteroatoms (i.e., benzene) are more stable than 5-membered rings or rings with heteroatoms.

3.2. *Fluidized Bed Data*

Doolan *et al.*[21] used quartz tubular reactors to study secondary cracking (i.e., reaction) of the tar vapors generated in a fluidized bed pyrolyzer. The cracking reaction temperatures were changed from 870 to 1370 K. Very little cracking occurred at 870 K. As the cracking temperature was raised, the light hydrocarbon yields increased rapidly. Products were predominantly alkenes, with smaller yields of methane and benzene. At higher temperatures, the light hydrocarbon yields passed through a maximum and eventually declined, while acetylene became the major product. The cracking reaction experiments were also conducted using a shock tube reactor. Products such as acetylene, benzene and carbon monoxide were observed. No carbon dioxide was produced from the cracking of the tar. Along with gases, liquid product defined as secondary tar, and solid product believed to be soot, were also observed. However, the yields of liquid and solid products were not reported separately.

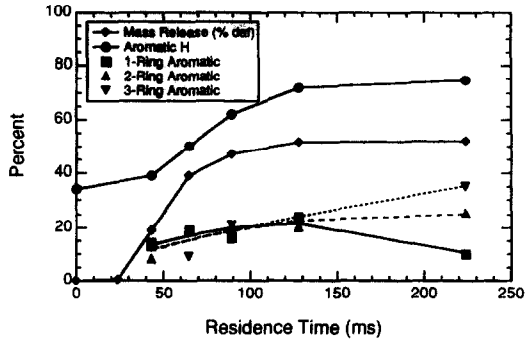

Fig. 2. Percentage of hygrogen contained in aromatic structure in tars from an Illinois no. 6 hva bituminous coal consisting of 1-ring, 2-ring, and 3- or more rings versus residence time for the 1250 K gas condition (from Pugmire *et al.*[22]).

3.3. *Entrained Flow Data in Inert Conditions*

The chemical structures of tars that experienced secondary reactions in nitrogen were examined using ^{1}H NMR and ^{13}C NMR by Fletcher *et al.*[12] and Pugmire *et al.*[22]. The pyrolysis experiments were carried out in an electrically-heated drop-tube furnace at 1050 and 1250 K. The collected tars showed increases in multiple-ring structures and decreases in aliphatic content as a function of residence time at 1250 K, as shown in Fig. 2. The increased hydrogen aromaticity of the tar most likely leads to the formation of soot nuclei. No such increases in hydrogen aromaticity or 3-ring structures were observed in coal tars collected as a function of residence time at 1050 K, indicating that secondary tar reactions become important between 1050 and 1250 K.

Freihaut *et al.*[23] used a flash lamp reactor to study tar evolution and secondary cracking for a bituminous coal. At low irradiance flux levels, only tar and low temperature decomposition gases were observed. At high irradiance levels, significant quantities of secondary decomposition product gases (HCN, C_2H_2, and CO) were observed. Freihaut and co-workers postulated that the high temperature cracking reactions may occur at the particle surface or in the particle–gas boundary layer.

Nenniger *et al.*[9,10] studied the sooting potential of several coals by separating aerosol from char particles after the pyrolysis of coals in a laminar flow furnace. The pyrolysis was carried out in an inert atmosphere of preheated argon. The separation system consisted of a virtual impactor in series with a cascade impactor. The separation efficiency was checked by SEM, but no quantitative efficiency measurement was conducted. The

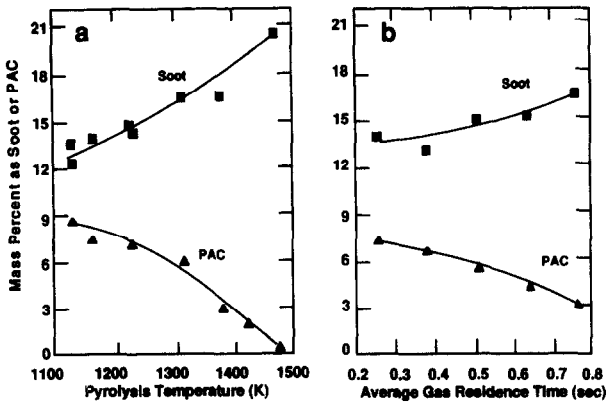

Fig. 3. Tar and soot (PAC) yields from a Pittsburgh seam hva bituminous coal obtained in a drop tube reactor in argon (a) vs. temperature at a residence time of 0.75 s, and (b) vs. residence time at 1375 K (from Wornat *et al.*[11]).

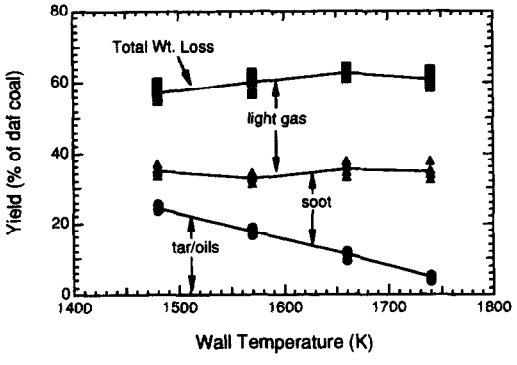

Fig. 4. Soot and tar yields obtained for Pittsburgh no. 8 hva bituminous coal in a radiant drop tube reactor (adapted from Chen *et al.*[7]). Particle temperatures are several hundred degrees lower than the wall temperature.

aerosol was believed to consist of extractable tar, soot and condensed ash. The tar yield was assumed to be the amount of the aerosol extractable with dichloromethane. The condensed ash content was determined from neutron activation analysis. The soot yield was calculated by difference. They found that the soot yield increased while the tar yield decreased as the pyrolysis temperature was raised. The sum of soot plus tar remained constant with increasing severity of pyrolysis. At a high temperature (2200 K), about 20 wt.% of a dry high-volatile bituminous coal was converted to soot. Soot inside char particles was also observed under TEM by crushing the char particles. This seems to suggest that the actual soot yields may be higher than indicated by the cyclone/cascade impactor system.

Wornat *et al.*[11] investigated changes in the composition of polycyclic aromatic compounds (PAC) from the pyrolysis of a high-volatile bituminous coal in argon. Overall, a loss in compositional complexity was observed as the severity of secondary reactions increased, suggesting the selective survival of a group of stable species. The stable species were identified as unsubstituted PAC. PAC reactivity followed the following order: aromatic amines > aromatic ethers ≈ multialkylated PAC ≈ phenols > monoalkylated PAC > unsubstituted PAC > carbonyl-substituted PAC. In other words, the compounds with more complex attachments were more reactive than compounds with simple or no attachments. For the high volatile bituminous coal studied, about 20 wt.% of the coal was converted to soot at high temperatures and long residence times. In addition, the sum of PAC and soot yields was relatively constant (supporting the findings of Nenniger *et al.*[9]), as shown in Fig. 3, suggesting that PAC serves as a precursor to soot.

Chen and co-workers[7,24,25] performed coal pyrolysis experiments in an inductively-heated radiant drop-tube furnace in an inert argon atmosphere. They also reported that the yields of tar/oils plus soot in the secondary pyrolysis experiments were constant and were equal to the tar-plus-oil yields obtained at the longest residence time in primary pyrolysis experiments (see Fig. 4). For a high-volatile bituminous coal at higher temperatures,

Table 1. A summary of coal pyrolysis soot yields measured in drop tube reactors in argon

Investigator	Nenniger[10]	Wornat *et al.*[11]	Chen[24]
Pyrolysis environment	Argon	Argon	Argon
Reactor	Drop-tube, electrically heated	Drop-tube, electrically heated	Radiant drop-tube
Pyrolysis temperature (K)	1300–2200	1130–1480	1480–1740*
Soot yield	Increases with T. Reaches a plateau	Increases with T and residence time	Increases with T and residence time
Tar yield	Decreases with temperature	Decreases with temperature and residence time	Decreases with temperature and residence time
(Soot + tar) yield	Remains unchanged	Remains unchanged	Remains unchanged

*Temperatures reported by Chen were reactor wall temperatures. The particle temperatures were several hundred degrees lower.

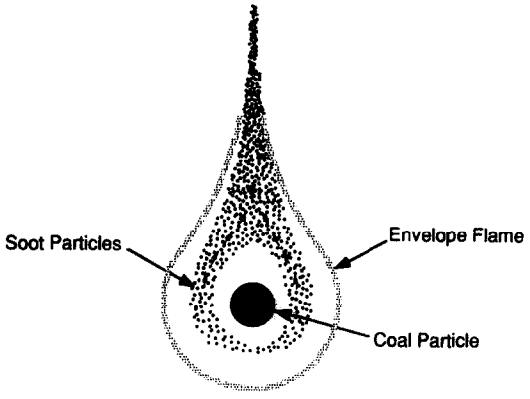

Fig. 5. Schematic representation of the formation of soot in the envelope flame surrounding a devolatilizing coal particle in the presence of oxygen (from Ma[13]).

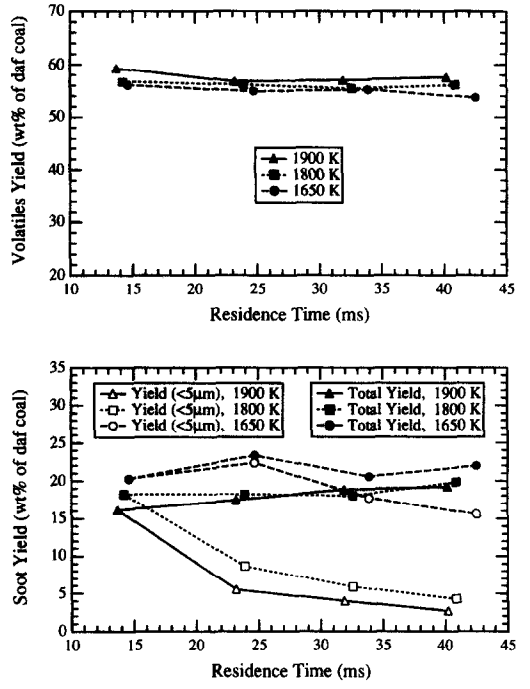

Fig. 6. Measured volatiles yields and soot yields in a fuel-rich flat flame reactor for Pittsburgh no. 8 coal[6,30].

more than 25% of the coal mass (daf) was converted to soot. For gas-phase products, C_3 hydrocarbons and ethane decreased monotonically with temperature, while methane and ethylene reached a maximum and then dropped. Acetylene increased dramatically during soot formation and growth.

The high soot yields reported by Nenniger *et al.*[9], Wornat *et al.*[11], and Chen[24] were all obtained in inert (argon) conditions. All three of these groups reported that the sum of tar plus soot remained constant in their experiments; increases in soot yield coincided with decreases in tar yield. The profiles of soot yield versus temperature in these coal pyrolysis experiments showed no decreases at increased temperatures; the soot yields either increased with temperature monotonically or reached an asymptotic value. Table 1 summarizes their experimental results.

3.4. *Coal Combustion Data*

Only a few studies have been performed on secondary chemistry of coal tar in oxidizing conditions. These studies show that in certain flame environments, oxygen-containing species will cause the destruction of PAH. Haynes[26] investigated the decomposition of pyrene injected into the post-flame gases ($T \sim 1700$ K) of near-sooting and slightly sooting ethylene/air flames at atmospheric pressure. In a very fuel-rich, sooting flame, no decomposition of the pyrene occurred over extended reaction times. At more fuel-lean flame conditions, significant decomposition of the pyrene occurred. It was argued that the pyrene decomposition was due to reaction with OH radicals.

Soot formation around an individual pulverized coal particle was observed by McLean *et al.*[15] using a methane/hydrogen/air flat flame reactor. For bituminous coals, ejected volatile matter formed a condensed soot-like phase, which was oxidized during the early stage of char burning under oxidizing conditions and that persisted throughout the reactor under reducing conditions. During lignite pyrolysis, a condensed phase was not observed, since lignite volatiles are largely composed of light gases instead of high-molecular-weight hydrocarbons. Seeker *et al.*[16] performed similar research using a down-fired methane/air flat flame, running in a lean (35% excess air) condition. They found that both particle size and coal rank affected the sooting tendency. For large bituminous particles (80 μm), a significant volatile fraction was ejected from the particle as a jet. This volatile jet reacted close to the particle, producing a trail of small solid particles believed to be soot. Tails of soot were not observed for lignite, anthracite, and small bituminous particles. A schematic representation of the formation of soot tails observed by McLean and co-workers and by Seeker and co-workers is shown in Fig. 5; soot particles formed in the particle boundary layer flow around the particle and agglomerate in the particle wake.

Timothy *et al.*[27] studied the formation and burnout of soot during the combustion of three high-volatile bituminous coals using a combination of high-speed photography and two-color optical pyrometry. Soot was observed to form in a nearly spherical shell displaced from the particle surface by one to four particle radii. The overall soot cloud diameter was approximately constant, but the shell thickness increased with decreasing oxygen concentration. The peak soot concentration ranged from 0.5% of the mass of coal (at oxygen concentrations greater than 50%) to 3% (at a lower concentration of 10% oxygen). Several models have also been developed to describe the volatiles flames around individual particles as a result of this type of single-particle combustion experiment[28,29]. In these models, thermophoresis and radiation account for the transport processes of soot near the particle.

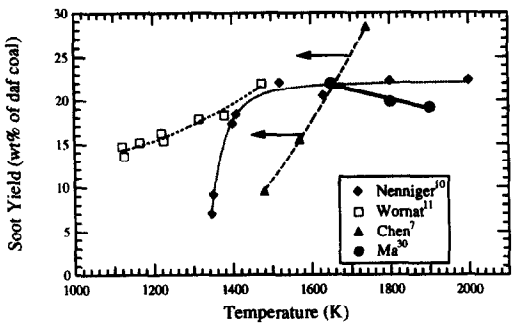

Fig. 7. Comparison of soot yield versus temperature for experiments in argon[7,10,11] vs. experiments in a fuel-rich flat flame reactor[13].

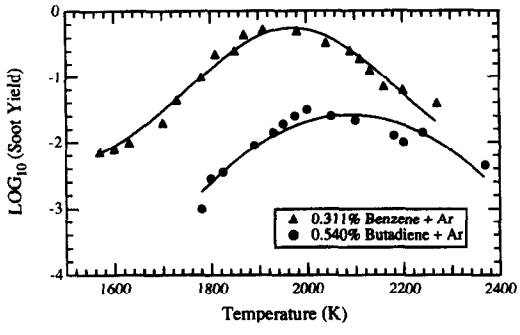

Fig. 8. Soot yields versus temperature for benzene and butadiene[31].

3.5. *Entrained Flow Experiments in Post-combustion Gases*

Ma and co-workers[6,13,17,30] measured soot yields from entrained-flow coal pyrolysis in a flat flame reactor. A $CH_4/H_2/O_2/N_2$ flame was operated under fuel-rich conditions to provide a high temperature oxygen-free environment to study soot formation and agglomeration. No soot was observed from the gas flame in the absence of coal particles. As shown in Fig. 6, the total volatiles yields remained relatively constant as a function of residence time for any given temperature condition. The slight increase in soot yield with residence time at the highest temperature condition is probably due to experimental error limitations. Ma reported the presence of soot agglomerates in the char sample that were larger than the 5-μm cutpoint diameter of the separation system. These large soot agglomerates were black, compared to the grayish color of the char particles, and were separated using a 38-μm sieve (the parent coal particle size was 63–75 μm). The large soot agglomerates did not contain mineral matter, and were examined by SEM to verify that they were separated from the char particles.

Ma and co-workers reported that the total soot yield did not change as a function of residence time, but that the yield of soot particles with sizes less than 5 μm decreased significantly with residence time at the higher temperatures, as shown in Fig. 6 for a Pittsburgh no. 8 coal. Since the amount of large agglomerates increased significantly as a function of residence time, the agglomeration did not appear to occur in the sampling probe. Other high-volatile bituminous coals exhibited the same behavior. The experiments was repeated using acetylene in place of the coal particles to see if the large agglomerates were formed from a fuel other than coal. The acetylene experiments only produced soot agglomerates smaller than 5 μm, as indicated in the literature. This suggests that coal pyrolysis products (i.e., tar) can result in soot particles with larger sizes than indicated by experiments with simple hydrocarbon fuels (such as acetylene). This may be due to the fact that primary coal tar is highly aromatic, with a molecular weight of ~350 Da, as opposed to simple hydrocarbons where the formation of the first aromatic ring is often a rate-limiting step. Tar molecules also contain side chains, which may also cause different soot formation characteristics than simple hydrocarbon fuels.

The total soot yields measured in the fuel-rich flat flame experiment[6,13] are compared with soot yields obtained in inert pyrolysis conditions[10,11,14] in Fig. 7 for Pittsburgh high volatile bituminous coals. Nenniger's data show that an asymptotic value was reached at increased temperatures. Wornat's data show depletion of tar at the maximum residence time, and hence her peak soot yield should be considered as an asymptote. The high yield obtained by Chen does not appear to be a limit, since a small amount of tar still exists at his peak soot condition. The data obtained by Nenniger, Wornat and Chen all show that soot yields increase or remain constant with temperature. One interesting result of the flat flame reactor data[13] is that the total soot yield decreased slightly with increased temperature. This result is different from the results of inert coal pyrolysis experiments, but is comparable with the results obtained in the hydrocarbon flame experiments or hydrocarbon pyrolysis experiments[13,31]. The soot yield in the hydrocarbon experiments always shows a bell-shaped profile when plotted against temperature, as shown in Fig. 8. At high temperatures, cracking reactions are favored over polymerization reactions, and soot yields decrease. The magnitude of soot yield decrease versus temperature observed in the coal experiments is much smaller than in the hydrocarbon experiments; this may be due to the high molecular weight of coal tar compared to 1-ring aromatic species.

The slight decrease in soot yield with increasing temperature in the flat flame reactor experiments can be explained by the stability of tar molecules at high temperatures and the reactions of tar by gaseous species existing in the post-flame region of the flat flame reactor. Polymerization and PAH cracking are competitive reactions in the soot formation process, and the stability of the high-molecular-weight PAH tends to decrease with temperature. On the high temperature side of the bell-shaped soot yield curve, increases in temperature favor the cracking reaction, which leads to a lower soot yield. The slight decrease in soot yield with increasing temperature in the flat flame reactor may be due to reactions of the oxygen-containing species, especially

OH and O radicals, with tar molecules and intermediate PAH. The concentrations of oxygen-containing radicals such as OH and O increase drastically with increases in temperature[13]. Because of the increased attack of PAH molecules by these radicals, the stability of PAH is reduced further. This could explain why the soot yields obtained at high temperatures in inert atmospheres were higher than the yields obtained in the post-flame gas environment, and should be considered in combustion calculations.

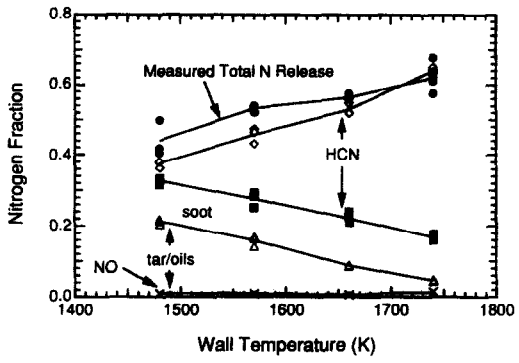

Fig. 9. Distribution of nitrogen during the pyrolysis of a Pittsburgh no. 8 hva bituminous coal in a radiant drop tube reactor[25]. Particle temperatures are several hundred degrees lower than the wall temperature in this experiment.

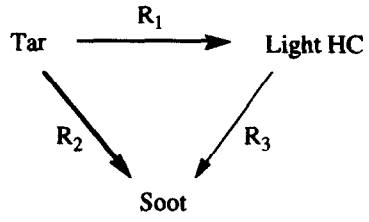

Fig. 10. Possible reaction pathways for soot generation in coal pyrolysis (suggested by Chen *et al.*[7]).

4. NITROGEN IN COAL-DERIVED SOOT

Several research studies have been conducted on the evolution of nitrogen in coal pyrolysis (e.g. [25,32–36]), and some reviews are available (e.g. [37,38]). Most of the research concentrated on the nitrogen distribution in tar, char and gas, and how the nitrogen-containing species were destroyed to form precursors of nitrogen oxides. HCN and NH_3 are believed to be the precursors of fuel NO_x. Regarding the effect of coal rank, some studies report that coal type and coal composition have little effect on the nitrogen distribution, while others argue that coal rank is related to nitrogen functionality, which determines the nitrogen evolution. Solomon and Colkett[33] conducted pyrolysis experiments on a heated grid for a lignite and 12 bituminous coals at low temperature, showing that initial nitrogen release occurred through the release of tar, while non-tar nitrogen release occurred at long residence times and/or high temperatures. Similar results from independent heated grid experiments also show the release of HCN only at higher temperatures ($> 1000°C$)[34]. The high-temperature HCN release is attributed to cracking of aromatic compounds, which occurs in both the char and in the tar.

The stability of fuel-nitrogen compounds with respect to secondary pyrolysis has been investigated in both coal pyrolysis[35] and model compound pyrolysis studies[39–41]. These studies revealed that the reactivities of pyrrolic type structures are greater than those of pyridinic type structures. It was also reported that the sooting tendency of pyridine was very low compared to that of benzene, although pyridine has considerable aromatic character[42]. However, only a few studies have been performed regarding the effect of soot on the evolution of nitrogen.

Wornat *et al.*[43] studied the changes in the ring number composition of nitrogen-containing polycyclic aromatic compounds (PACN) and soot nitrogen during pyrolysis. They found that the mass distribution and rate of decay of the PACN followed the order: 5-ring > 6-ring > 4-ring > 3-ring > 2-ring. It was also found that the PAC conversion reactions leading to ring build up, ring rupture, and soot formation were faster for PACN relative to the nonpolar PAC, because C–N bonds within the aromatic rings in the coal were weaker than the C–C bonds. Elemental analysis also showed that the N/C ratio in the soot dropped with increasing PAC conversion. The percentage of coal nitrogen evolved in soot declined with the increase of pyrolysis severity, while the soot yield increased. It was postulated that this decline in soot nitrogen content was due to (a) nitrogen liberation from the soot generated, and (b) soot growth resulting from the conversion of PAC with successively lower nitrogen content.

Chen *et al.*[7] examined soot and nitrogen evolution in coal pyrolysis in a drop tube reactor operated in the radiant heating mode. Their experimental results showed that tar aromaticities increased dramatically, reaching ultimate values greater than 0.67. The C/H mole ratio in the soot changed from 2 to 10 when residence time was increased. Up to one-fourth of the coal-nitrogen expelled in volatiles during primary devolatilization was incorporated into soot during secondary pyrolysis for coals whose volatiles were dominated by tar. Ten percent of the volatile nitrogen for a sub-bituminous coal was incorporated into soot. Nitrogen incorporation into soot occurred early in the secondary pyrolysis process, and the total amount of coal-nitrogen in soot remained constant even when soot yields were observed to increase dramatically with increases in residence time, as shown in Fig. 9. Additional data on nitrogen in soot are available[6].

A global mechanism of soot formation was proposed by Chen *et al.*[7], as shown in Fig. 10. Here, all reaction pathways are irreversible. In earlier stages, R_2 is the major pathway for soot formation, and nitrogen-containing compounds are incorporated in soot. Thereafter, substantial soot mass is added via R_3. Direct tar addition

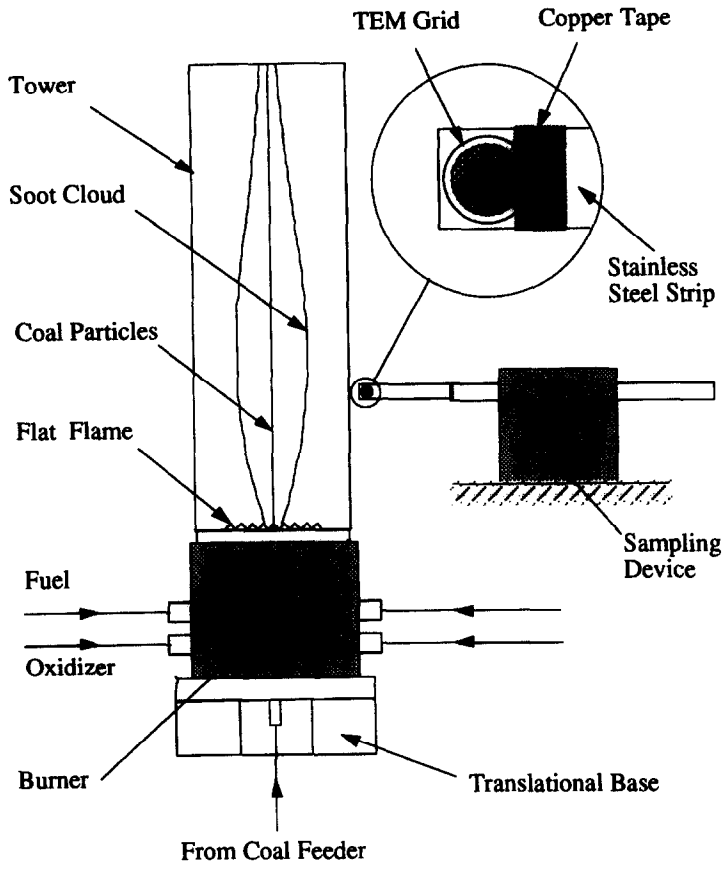

Fig. 11. Schematic of the flat flame flow reactor and thermophoretic sampling system (from Ma *et al.*[17]).

to soot in later stages is possible only if tars eliminate their nitrogen before being added to the soot.

The fact that coal-derived soot contains nitrogen implies that coal-derived soot must be examined for (a) the contribution to near-burner heat transfer, and (b) the contribution to the transformation of nitrogen in the fuel to NO_x and its precursors.

5. SOOT PARTICLE/AGGLOMERATE SIZE

Soot formation is a very complicated process involving hundreds of elemental steps. Qualitatively, there are three stages that lead to a primary soot particle: (a) particle inception or nucleation; (b) surface growth; and (c) coagulation[1]. After these three stages, however, the primary particles may continue to undergo (d) agglomeration and (e) aggregation processes[9]. During *particle inception*, the first condensed-phase material arises from the fuel molecules and their oxidation or pyrolysis products. Such products typically include various unsaturated hydrocarbons, especially acetylene and PAH. These two types of molecules are often considered the most likely precursors of soot in flames. Once the first particles are formed, the soot loading (the mass of soot per unit volume) can be increased by *surface growth*, which involves the attachment of gas-phase species (mainly acetylene) to the surface of a particle. Surface growth reactions lead to an increase in the amount of soot, but leave the number of particles unchanged. *Coagulation* also leads to particle growth, where particles collide and coalesce. Although the number of particles is decreased, the soot volume fraction remains constant during the coagulation process. At later stages in the growth process, particles no longer coalesce on collision, but are chemically fused together in chains. Primary particles are discernible in the chains. The growth by non-coalescent collision is known as *agglomeration*. Usually, agglomerates can subsequently become entangled with other agglomerates through a process known as *aggregation*.

5.1. *Optical Experiments*

Using high magnification shadowgraphs, McLean *et al.*[15] observed that volatile matter undergoes polymerization reactions to form a soot-like condensed cloud around single combusting coal particles. McLean's experiments were conducted in a flat flame methane–air reactor with 8% post-flame oxygen. They suggested that the condensed cloud consisted of small soot particles called soot nuclei. Primary soot particles are much smaller than coal or char particles, and therefore travel at the gas velocity rather than the particle velocity, as does the tar cloud. Soot nuclei undergo surface growth as surrounding organic matter adheres to the soot surfaces.

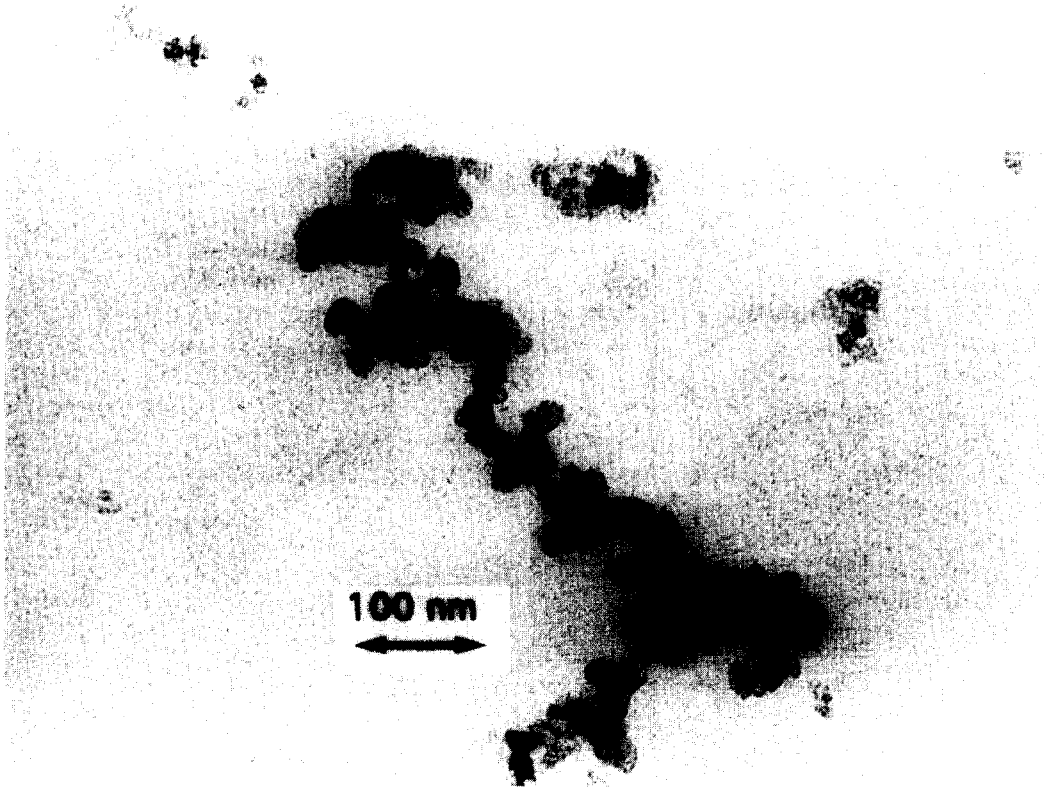

Fig. 12. TEM micrograph of soot from the Utah coal, collected at 13 cm above the burner (65 ms) (from Ma *et al.*[17]).

In McLean's experiment, the soot particles impact each other in the vicinity of the coal particle and coalesce to form agglomerates, which are generally in the form of long rod-like structures. As soot travels around the coal particle in the Stokes flow regime, soot particles form agglomerates in the form of streamers, as illustrated in Fig. 5. These rods or "tails" were observed by McLean and co-workers to be as long as 500 μm, but only about 40 μm in diameter. The average initial coal particle diameter in McLean's experiments was 65 μm. The initial soot particles formed did not escape the vicinity of the particle during devolatilization due to the surrounding volatiles flame. The temperature gradient between the flame and the coal particle surface is a thermophoretic driving force that pushes soot particles back towards the surface. Also, soot particles that travel through the flame are oxidized. Therefore, in the single-particle coal combustion experiments (with O_2 present) examined by both McLean *et al.*[15] and Seeker *et al.*[16], most of the soot is observed in large agglomerates in the form of streamers.

5.2. *Thermophoretic Sampling Experiments*

Ma *et al.*[17] performed thermophoretic sampling of soot particles formed during high-temperature coal devolatilization in order to examine soot particle sizes and shapes. A schematic of the thermophoretic sampling device used in a fuel-rich flat flame reactor is shown in Fig. 11[17]. The soot formed from the coal pyrolysis products formed a cloud that expanded radially away from the stream of char particles along the reactor centerline, facilitating sampling experiments in the soot cloud without contamination by char particles. A carbon-coated microscope grid was briefly inserted into the soot cloud (residence time of 0.1 s), where the temperature gradient between the soot particles and the cold grid surface caused the migration of soot particles and resulted in deposition. Soot particles were analyzed using transmission electron microscopy. Distinct primary soot particles with approximate diameters of 25–60 nm were observed, along with agglomerates composed of multiple primary particles. Condensed, highly volatile, liquid-like deposits were observed in some cases, which was thought to be tar at some stage of secondary reaction. A representative soot agglomerate from the thermophoretic sampling experiments is shown in Fig. 12. Agglomerates were also observed with characteristic dimensions of as high as 800 nm, some of which showed the presence of carbon tubes rather than carbon spheres. However, only qualitative results were obtained in these thermophoretic sampling experiments; no definitive trend was observed with residence time.

5.3. *Bulk Solid Sampling Experiments*

Size determination of soot samples is difficult with the bulk solid sampling experiments. Some limited data were obtained by Nenniger[10] using a cascade impactor

collection system. The experiments performed in a fuel-rich flat flame reactor[6,13,17] have shown the potential for generation of large soot agglomerates (5–38 μm in diameter) in the presence of post-flame gases (e.g., H_2O, CO_2, OH, etc.). However, the exact mechanism for formation of such large soot particles, which has not been seen in soot formation experiments for simple hydrocarbons, remains to be determined.

6. OPTICAL PROPERTIES OF SOOT

The optical properties of coal-derived soot have not received as much attention as soot derived from gaseous hydrocarbon fuels. The reason for this neglect may be the difficulty in separating the radiation effects of coal-derived soot, char, and flyash. The radiative properties of coal-derived soot have not been characterized, nor have the influences of coal type, volume fraction and morphology been examined.

Optical properties of a material can be defined by many different variables. The most fundamental is the complex index of refraction. The complex index of refraction has a real and an imaginary component. The real component is the ratio of the speed of light in a vacuum to the speed of light within the particle. The imaginary component is a measure of the attenuation of light within the particle. Other key optical variables often used in radiation calculations are (a) the scattering and absorption coefficients and (b) the scattering phase function[44]. Different combinations of these data are presented in the literature.

The radiative properties of coal-derived soot can be used in combustion modeling and burner design. In the near-burner region, the stoichiometry is very fuel rich providing for a high soot volume fraction and for large radiative heat fluxes being transmitted to the burners and walls. In this region, neglecting soot can result in inaccurate radiant flux predictions, as well as inaccurate predictions of gas temperatures, species concentrations, pressure fields, and velocity profiles. Radiative properties of soot can also be used to perform in situ measurements of soot volume fraction and soot temperature. Known radiative properties provide means for data reduction of emission–transmission measurements. Previously, data from soot derived from gaseous hydrocarbon fuels have been used in coal combustion calculations. Some researchers[6,13,17,45,46] have suggested a correlation between the fuel hydrogen/carbon (H/C) ratio and the radiative properties of soot from gaseous fuels. Others claim that spectral radiative properties of soot are insensitive to the parent fuel[47]. There have also been indications that residence time in the flame affects the radiative properties of soot[47–49].

While research has concentrated on the optical properties of soot from gaseous hydrocarbon fuels and plastics, there has been little work done on soot from coals. The only work reported is a correlation for the gray absorption coefficient of coal-derived soot[50]. This correlation quotes a reference from Gray and Muller[51] that calculates a range of empirical constants for use in an absorption coefficient relation for coal flames. These calculations were based on reflection data from graphite and coal, not from coal-derived soot data[52]. No work has been presented on the complex index of refraction or absorption coefficients of coal-derived soot[5] and no experimental comparison has been made between the soot derived from gaseous hydrocarbon fuels and that derived from coal combustion.

Due to the short expected lifetime of soot in flames, and since soot is thought to exist only in the near-burner region, it is claimed that soot does not affect the overall heat transfer in a coal-fired furnace[5]. However, the portion of the flame where soot exists is of extreme interest to combustion modelers and burner designers. Radiation from soot can greatly increase heat flux to the burner surface since the soot has a large surface area and high temperature compared to the larger coal and char particles. This heat flux to the burner surface must be removed by cooling to avoid damage to the burners. Further, the large radiant capacity of soot can locally affect gas temperature profiles in regions where prediction of temperature-sensitive pollutant formation and particle ignition are important. Radiative heat transfer feedback to the fuel stream may also affect devolatilization and ignition.

The radiative distribution of heat flux from a black body shows that the peak radiative flux occurs at 2898 μm K. This value is the product of the temperature of the body and the wavelength of radiation. At a typical peak coal-fired boiler temperature, 2000 K, this peak wavelength occurs at 1.45 μm. According to the Planck blackbody distribution[53], 75% of particle radiation occurs at infrared wavelengths greater than the peak wavelength[54]. The high percentage of emission in the infrared makes accurate measurements of soot optical properties very important in this region.

The optical properties of coal-derived soot may differ from gaseous hydrocarbon soot due to the difference in chemical constituents of the coal and gaseous hydrocarbon fuels. No data have been published yet on this subject. Various experiments measured the precursors to soot and the yield of soot from coal combustion[7,9,11,24,25], but none reported optical properties.

There are several parameters that are seen as important in determining the optical properties of soot particles: (1) the temperature of the soot; (2) the C/H ratio of the soot and of the fuel; (3) the size of the primary particles; and (4) the size and shape of agglomerates. Each of these areas of interest has been explored by various researchers.

Given the dearth of experimental data for radiative properties of coal-derived soot, one must draw from published data and techniques used to model soot from simple gaseous hydrocarbon fuels. The following sections summarize research on soot from hydrocarbons that may be related to coal-derived soot. It should be noted, however, that the difference in chemical structure between the chemical structure of coal- and

Table 2. Optical property measurements of soot and graphite using the reflection technique

Researcher	Date	Carbon type/fuel	Wavelength	Angles	Data	S
Senftleben and Benedict[62]	1918	Electrode black	Visible, IR	58–66°	n_λ, k_λ, R	P
McCartney and Ergun[52]	1958	Graphite	Visible	all at 20°	n, k, R	C
Taft and Philipp[61]	1965	Graphite	UV, Vis., IR	normal	R_λ	C
Foster and Howarth[45]	1968	Graph., C. black	Visible, IR	60–80°	n_λ, k_λ, R	P, C
Dalzell and Sarofim[63]	1969	Propane, acet.	Visible, IR	45°	n_λ, k_λ	P
Tomaselli *et al.*[66]	1981	Graph., C. black	IR	3 angles	n_λ, k_λ	P
Felske *et al.*[59]	1984	Propane	Visible, IR	5–80°	n_λ, k_λ, R	P
Batten[64]	1985	Propane, keros., acet., C. black	Visible	20–80°	n_λ, k_λ	P
Stagg and Charalampopoulos[65]	1993	Propane, graphite	Visible	all at 20°	$n_\lambda(T)$ $k_\lambda(T)$	P, C

Table 3. Optical properties of graphite and soot measured by *ex situ* extinction

Researcher	Date	Soot type/fuel	Wavelength	Technique	Data
Millikan[67]	1961	Acet., ethylene	Visible	*Ex situ* extinction	α
Siddall and McGrath[68]	1963	Various soots	IR	Soot layer	α_λ
Yasinsky and Ergun[69]	1965	Graphite	IR	Ultrathin flake	τ_λ, ω, g
Chippett and Gray[70]	1978	Acetylene	Visible	Fluid suspension	κ_λ
Janzen[57]	1979	Carbon black	Visible	Fluid suspension	n, k
Ku[71]	1982	Propane, C. black	Visible, IR	Fluid suspension	n_λ, k_λ

gaseous-derived soot raises questions as to the applicability of these gaseous soot data to coal flames.

6.1. Ex Situ *Measurements*

Most early attempts at determining refractive index of soot particles involved *ex situ* reflection measurements at various angles to the surface of graphite or soot. These surfaces were prepared by freshly cleaving a graphitic structure to make a smooth surface or by compressing soot in a high pressure die to form a small smooth pellet. Reflection techniques use the Fresnel equations to deduce the complex index of refraction. A frequently used technique developed by Avery[55] uses the reflectivity of polarized light at two different angles to calculate the complex index of refraction. Other reflection techniques use unpolarized light.

Disagreement about published reflection data come from concerns that pellet surfaces are not adequately smooth and therefore do not satisfy the Fresnel conditions[56,57]. An additional concern is that when soot is compressed to very high pressures, there are still significant void fractions of air in the pellet (up to 1/3 by volume)[57–59]. Since pellets are a mixture of soot and air, and pellet properties may not accurately reflect the properties of a voidless solid soot sample. A final concern, raised as a criticism of all *ex situ* measurements, is that the properties measured at room temperature may be different from the properties of soot at flame temperatures[60].

Reflection measurements have been performed in the ultraviolet[61], the visible[45,52,59,61–65] and the infrared[45,59,61–63,66] as summarized chronologically in Table 2. Investigators, the year of the study and the type of carbon are listed in the first three columns. The other columns list the wavelength region of interest, the angles at which reflectance measurements were taken, and the data presented. In the data column n and k represent the real and imaginary parts of the complex index of refraction and R represents the reflectivity (the ratio of reflected to incident light). The final column lists the type of surface preparation (S). A compressed pellet is denoted with P and a cleaved surface is denoted with a C.

There are several other techniques that can be used to make ex situ measurements of soot optical properties. These include: (1) extinction techniques through an ultra-thin layer of graphite or soot[67–69]; (2) dispersion of a soot sample in liquid[57,70,71]; and (3) dispersion of a sample in a KBr pellet. These techniques and reported data are summarized in Table 3. The variable α_λ[67,68] shown in Table 3 is defined by:

$$\tau_\lambda = I_\lambda / I_{\lambda,0} = e^{-c\lambda^{-\alpha_\lambda} L}, \tag{1}$$

where $I_\lambda/I_{\lambda,0}$ is the ratio of incident to transmitted light at a given wavelength (λ), L is the path length, λ is the incident wavelength and c and α are constants. The variables reported by Yasinsky and Ergun[69] were transmittance, τ, and the dispersion constants, ω and g. These extinction techniques, like the other *ex situ* techniques, are limited in that measurements are made at room temperature, that the morphology of the soot may be different than in flame conditions, and that it is extremely difficult to accurately measure sample path lengths for many of these techniques.

6.2. In situ *Measurements*

There are three basic forms of *in situ* measurements of soot optical properties. These are extinction, emission and scattering measurements. Combinations and perturbations of these methods fill the literature[46,48,49,70–81]. The data from *in situ* measurements are reported in Table 4. The researchers reported their results with various variables and assumptions. Some of the key

Table 4. *In situ* optical property measurements of soot and graphite

Researcher	Date	Soot type/fuel	Wavelength	Method	Data
Erickson *et al.*[72]	1964	Benzene	Visible	Scattering	Scat
D'Alessio *et al.*[73]	1973	Methane	UV	Scattering	α_λ
Buckius and Tien[74]	1977	Polystyrene, Delrin, Plexiglass	IR	Emission, transmission	Rad, τ, κ_λ/f_v
Chippett and Gray[70]	1978	Acetylene	Visible	Extinction	β_λ, n_λ, k_λ
Bard and Pagni[75]	1981	Acetylene	Visible	Extinction	β_λ
Powell and Zinn[76]	1983	Smoke	Visible	Scattering, extinction	Q_e, n, k
Ben Hamadi *et al.*[77]	1987	Propane, methane	Visible, IR	Emission, transmission	$\beta_\lambda L$, Rad, α
Charalampopoulos and Felske[48]	1987	Methane	Visible	Scattering, extinction	Q_e, n, k
Charalampopoulos and Chang[49]	1988	Propane	Visible	Scattering, extinction	$Q_{\lambda,e}$, n_λ, k_λ
Habib and Vervisch[46]	1988	Ethylene, methane, propane	Visible, IR	Extinction	$\beta_\lambda L$, n_λ, k_λ
Solomon *et al.*[78]	1988	Coal-derived soot	IR	Emission, transmission	Rad, τ_λ
Sivathanu *et al.*[79]	1993	Methane, propane, ethylene	IR	Emission, transmission	κ_λ/f_v
Koylu and Faeth[80]	1994	Acetylene, propane, propylene, ethylene	Visible, near IR	Scattering, extinction	$CS_{\lambda,s}$, $CS_{\lambda,e}$
Koylu and Faeth[81]	1994	Ethylene, acetylene	Visible	Scattering	CS_s

Table 5. Dispersion constants for soot

Electron type	Fuel	Electron number density, N (m^{-3})	Resonant frequency, ω (rad s^{-1})	Damping constant, g (rad s^{-1})
Dalzell and Sarofim[63]	Propane			
Bound 1		2.69e27	1.25e15	6.0e15
Bound 2		2.86e28	7.25e15	7.25e15
Free ($m_f = m_b$)		4.06e27	–	6.0e15
Lee and Tien[60]	Plexiglass and polystyrene			
Bound 1		4.07e27	1.25e15	5.9e15
Bound 2		4.47e28	7.25e15	5.6e15
Free ($m_f = m_b/18$)		4.00e25	–	1.2e15
Charalampopoulos and Chang[49]	Propane			
Bound 1		3.88e27	1.25e15	9.8e15
Bound 2		4.26e28	7.25e15	6.1e15
Free ($m_f = m_b/18$)		4.82e25	-	1.2e15
Habib and Vervisch[46]	Propane and methane			
Bound 1		1.67e27	1.25e15	7.0e15
Bound 2		1.83e28	7.25e15	7.25e15
Free ($m_f = m_b/18$)		7.00e24	–	1.2e15
Habib and Vervisch[46]	Ethylene			
Bound 1		3.34e27	1.25e15	7.0e15
Bound 2		3.66e28	7.25e15	7.25e15
Free ($m_f = m_b/18$)		1.40e25	–	1.2e15

variables used were: β (the extinction coefficient); κ (the absorption coefficient); Scat (the intensity of scattered light); Rad (the radiant flux emitted from the flame per solid angle at a given wavelength); Q (the efficiency); CS (the cross-section); and τ (transmittance, or the ratio of transmitted to incident light).

6.3. *Modeling of Optical Constants*

Even with all of the data obtained by various *in situ* and *ex situ* techniques there is a need to extrapolate the data outside specific measured regions. A useful theory was developed by Lorentz[82] near the beginning of the 20th century in which he described the electrons in matter as a series of simple harmonic oscillators. These oscillators are acted upon by a local electromagnetic field that provides the driving force for their motion. The oscillators resonate at certain frequencies. The amplitude of this resonation is controlled by an effective damping constant that is related to the interaction of the electron with the material. If the material is nonconductive, this model represents the behavior of material subject to radiation. However, there are some deficiencies in this model if the material is a semiconductor or conductor. Since carbon can be treated as a semiconductive material and is the main constituent in soot, a modification to the Lorentz model was necessary to account for the physical properties of soot. A model that accounts for the free movement of electrons was developed by Drude[83]. By combining the Lorentz and Drude models a new model that accounts for the bound and free electrons in soot was possible. This model has the form of the summation of contributing factors for each of the bound and free electrons.

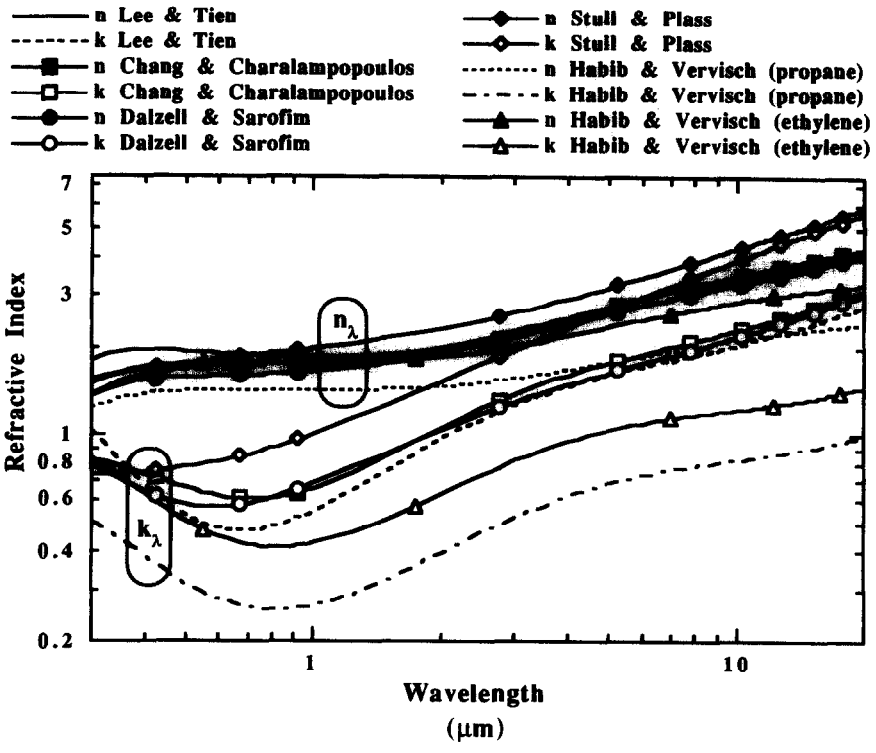

Fig. 13. Comparison of refractive indices using the dispersion model (from Rigby[85]).

The equation and theory of this combination model are described extensively[83]. The equation for the complex dielectric function, ϵ, of a material with both free and bound electrons can be written as:

$$\epsilon = 1 - \frac{\omega_{pf}^2}{\omega^2 + ig_f\omega} + \sum_j \frac{\omega_{pbj}^2}{\omega_{bj}^2 - \omega^2 - ig_{bj}\omega}. \quad (2)$$

where ω_p is the plasma frequency, defined as:

$$\omega_p^2 = \frac{Ne^2}{m\epsilon_o} \quad (3)$$

This function has a unique relation to the complex refractive index of a material, m:

$$\epsilon = m^2 = (n - ik)^2 \quad (4)$$

The real part, ϵ', and imaginary part, ϵ'', of ϵ can be directly related to the complex index of refraction. The relationships are shown explicitly below:

$$\epsilon' = n^2 - k^2 \quad (5)$$

$$\epsilon'' = 2nk \quad (6)$$

When Eq. (2) is divided into its real and imaginary components, and using Eq. (3), Eq. (5) and Eq. (6), the following equations result[60]:

$$n^2 - k^2 = 1 - \frac{e^2}{m_f\epsilon_o}\frac{N_f}{(\omega^2 + g_f^2)} + \frac{e^2}{m_b\epsilon_o}\sum_j \frac{N_{bj}(\omega_{bj}^2 - \omega^2)}{(\omega_{bj}^2 - \omega^2)^2 + \omega^2 g_{bj}^2} \quad (7)$$

$$2nk = \frac{e^2}{m_f\epsilon_o}\frac{N_f g_f}{\omega(\omega^2 + g_f^2)} + \frac{e^2}{m_b\epsilon_o}\sum_j \frac{N_{bj}\omega g_{bj}}{(\omega_{bj}^2 - \omega^2)^2 + \omega^2 g_{bj}^2} \quad (8)$$

These equations relate: ω (the frequency of incident radiation); ω_{bj} (the natural frequencies of the bound electrons); N (the density of each type of electron); e (the charge of an electron); m (the mass of an electron); g (the relaxation or damping frequency); and ϵ_o (the dielectric constant). The subscripts b and f represent the bound and free electrons, respectively, and the j subscript indicates the number of the bound electrons. From these equations it can be seen that there are several known variables and several unknown variables. The frequency of incident radiation ω is an input variable. The values of ϵ_o, e, and m are constant values that are known. However, the other variables need to be determined based on theory or measurements. For comparison, the dispersion constants from four studies are displayed in Table 5. Different researchers used different values for the effective mass of free electrons, as noted in the table. The mass of bound electrons were always taken as 9.1094×10^{-31} kg.

The dispersion constants in Table 5 have been used to make predictions for the complex index of refraction between 0.3 and 20 μm. A comparison between the predicted values of the complex index of refraction is shown in Fig. 13.

It can be seen that there exists disagreement on the optical properties of soot. In the area of coal-derived

soot, radiative property data are essentially nonexistent. In order to accurately model coal combustion this void needs to be filled. This is especially important when examining burner designs and pollutant formation. Previously, coal-derived soot optical properties have been assumed to be identical to the optical properties of soot derived from gaseous hydrocarbon fuels. Data analysis and comparison between soot from coal and from gaseous hydrocarbon fuel needs to be performed in order to verify or repudiate this assumption.

Preliminary ex situ measurements of the optical properties of coal-derived, propane-derived, and acetylene-derived soot show trends for optical properties of soot that differ as a function of residence time in a post-flame environment[84]. Values of the spectral absorption index ($C_\lambda = \kappa_\lambda \lambda / f_v$) increased as a function of residence time in a flow reactor for the propane-derived and acetylene-derived soot, whereas C_λ generally decreased with residence time for coal-derived soot[85]. Values of C_λ for three different coals were measured and compared, indicating trends as a function of coal type and residence time. The differences in optical properties of the coal-derived soot versus soot from propane or acetylene is likely related to the observed differences in the carbon and hydrogen contents of the respective soot samples[85]. Further work is needed to examine why coal-derived soot differs from soot derived from simple hydrocarbon gases, and to further explore the observed trends in optical properties for soot samples obtained from different types of coal. Explanations of why the optical properties of soot change as a function of residence time, as well as parameters to characterize these changes, are also needed.

7. MODELING OF SOOT FORMATION AND OXIDATION

The radiative transfer equation (RTE) is generally used to solve radiation problems in a semi-transparent medium. The RTE is an integro-differential equation which is most often solved by simplifying the radiative properties through physical models and then solving the equations using numerical methods. Additionally, solutions to the RTE require local radiative properties as input, such as the absorption coefficient, scattering coefficient, and scattering phase function. Detailed information on properties and characteristics of soot is difficult to obtain. For this reason, soot has not generally been included with the radiation model for the gases, particles, and surfaces in comprehensive coal combustion models.

Unagglomerated soot is generally small enough to be treated as non-scattering. This occurs when a particle is in the Rayleigh scattering regimen, or in other words, when the ratio of the circumference to the incident wavelength of light (the size parameter) is less than 0.3[50]. If a minimal number of agglomerates are present, thermal radiation from soot is due primarily to emission and absorption, which greatly simplifies radiation calculations. Therefore, it is generally assumed that no agglomerates are present when modeling soot radiation. The spectral absorption coefficient is used to describe absorption in a gaseous medium within the RTE. For most gases, this value has been measured by simply passing a length of monochromatic light through a container of a gas with a known density. This has not been done accurately for soot because the soot in the flame is not a gas, and is not easily captured and suspended. A frequently referenced, simplified method for estimating the absorption coefficient of soot has been developed[85]:

$$\kappa_\lambda = \frac{C_\lambda f_v}{\lambda} \tag{9}$$

In this equation, C_λ is a constant developed from Mie theory for spheres which is dependent on the complex index of refraction, f_v is the volume fraction of soot, and λ is the wavelength of the radiation. Sarofim and Hottel[86] developed a simpler model for the determination of the emissivity of soot disregarding the spectral effects. Their gray gas assumption is:

$$\epsilon_{soot} = 1 - (1 + 350 f_v T L_e)^{-4} \tag{10}$$

For an isothermal, homogeneous system, the emissivity may be related to the absorption coefficient through Bouguer's law:

$$k_{soot} = \frac{1}{L_e} \ln(1 - \epsilon_{soot}) \tag{11}$$

to give:

$$k_{soot} = \frac{4}{L_e} \ln(1 + 350 f_v T L_e) \tag{12}$$

where ϵ_{soot} is the emissivity of soot, T is temperature in Kelvin, and L_e is the mean beam length in the furnace.

Several researchers have indicated that approximate values of C_λ for most soot ranges from 3 to 7[87]. A recent comparison of optical properties of soot measurements taken from several different researchers shows significant variability[44]. Recent measurements by Majidi *et al.*[88] using soot from gaseous hydrocarbons and by Rigby and co-workers[84,85] using coal-derived soot have indicated that the optical properties for soot may vary significantly depending on the chemistry of the fuel of origin. Preliminary *ex situ* measurements of C_λ were affected by both residence time and fuel type (propane-derived soot versus coal-derived soot)[84,85]. This implies that an accurate estimation of the soot radiative properties may require detailed information regarding the chemistry of the soot, which is currently unavailable and beyond the scope of most practical modeling efforts. In the absence of exact soot radiative properties information, simplifying assumptions need to be made.

While accurate descriptions of soot radiative properties are important to obtain accurate soot radiation predictions, obtaining accurate soot volume fractions is even more critical. While typical values of C_λ range

from 3 to 7, typical values of f_v for radiating soot clouds range from approximately 10^{-8} to 10^{-6} (two orders of magnitude). It can easily be seen through Eq. (9) that accurate predictions of soot volume fraction are essential to the prediction of absorption coefficients.

Soot is thought to exist in the largest quantities in the fuel-rich region of flames. Efficient flames will burn off the soot, leaving little or no soot outside of the flame region. Several variables are thought to affect the soot volume fraction. In gas flames, acetylene is understood to be a precursor to soot. Unlike gas flames, soot in coal flames is thought to mostly evolve directly from the tar released from the coal during devolatilization. Similar to gas-derived soot, coal soot then undergoes oxidation, surface growth, and agglomeration.

Recently, Adams[89] and Adams and Smith[90] developed a simple empirical model for soot formation from coal that related the soot volume fraction to the local equivalence ratio. This model was applied in a simulation of a turbulent coal combustor. Soot was assumed to exist where the local equivalence ratio was 1.0 and above, increasing linearly to a maximum value at an equivalence ratio of 2.0 and above. The maximum soot value was calculated as a direct function of the amount of volatile carbon calculated to exist at that point. The soot volume fraction was then related to the radiative properties using Eq. (12). Turbulence effects were modeled using the assumed-shape PDF model[91]. Adams and coworkers reported that the inclusion of a soot radiation model increases predicted radiative transfer. However, the maximum local temperature difference between predictions of a turbulent coal combustion system, with and without the soot model, was only 50 K. This small temperature effect was thought to be caused by absorption of radiant heat by cold soot eddies near the hot soot eddies.

More sophisticated models have been developed for gaseous hydrocarbon flames. Frenklach[92] developed a model for hydrocarbon flames using detailed kinetics to describe soot formation. Frenklach's model includes 337 reactions and 70 species. Leung *et al.*[93] developed a more simplified kinetics model with 111 reactions. While kinetics mechanisms can be quite accurate, these methods are computationally intensive, which severely restricts use in current comprehensive modeling codes.

More complex models for two-dimensional laminar gas diffusion flames using the conservation equation for the volume fraction, including nucleation, surface growth, and oxidation source terms have been developed[94–96]. Other researchers have recently used variations of this model by solving transport equations for nucleation and the mass fraction of soot, which may be related to the volume fraction by assuming an average soot density. This involves the derivation of estimates for the nucleation, surface growth, and oxidation terms[95,97,98]. In a study by Coelho and Carvalho[99], two different soot formation submodels were coupled with three different oxidation submodels taken from different researchers in an effort to determine which models correspond best to measured data for turbulent gaseous flames. These submodels were combined with a model to solve the transport equations for the number density and concentration of soot. Predictions of soot in a turbulent propane diffusion flame were performed with the various combinations of models and compared with measured data. Recently, this method has been applied to a turbulent 3-dimensional flame[100]. In all of these studies, reasonable agreement existed between measured and predicted soot volume fractions. None of these advanced submodels have been applied to coal combustion systems; an improved model of soot formation and radiation in coal combustion systems is currently the subject of research[101,102].

Future work in the modeling field should involve the determination of more accurate radiative properties of soot as a function of fuel type. Large soot agglomerates of soot may scatter, which greatly complicates prediction of radiation effects. Accurate models may require a mechanism for determining particle size in addition to mass or volume fraction in order to estimate scattering effects. Improvements in turbulence modeling capabilities and solution methods for the RTE may be other research areas that impact the accuracy of soot models.

8. CONCLUSION

Only limited data have been collected on the yield of soot from coal and the properties of coal-derived soot. Soot yields from coal have only been measured in pyrolysis experiments, not in actual combustors. The yield of soot plus tar has been shown to remain constant in drop tube pyrolysis experiments in argon, regardless of the temperature. The soot yield was found to decrease slightly with increases in temperature in pyrolysis experiments in the post-flame environment of a fuel-rich (i.e., oxygen-free) flat flame reactor. This indicates that the composition of the surrounding gases may affect the transformation of tar to soot.

Primary soot particle diameters generated from coal are in size range of 25–60 nm. In pyrolysis experiments, where the soot escapes the immediate vicinity of the particle, soot particle agglomerates as large as 800 nm have been collected thermophoretically. Bulk sampling experiments in the flat flame reactor showed the presence of a significant amount of soot agglomerates that were larger than 5 μm but smaller than 38 μm. These large soot agglomerates were not formed when coal particles were replaced by a stream of acetylene. Single-particle combustion experiments in a flat flame reactor showed the formation of a soot tail in the wake of the char particle. The soot tails were up to 500 μm long in contrast to the initial coal particle size of 60–85 μm. These soot tails are thought to form by the thermophoretic forces acting on the soot particles between the particle surface and the envelope diffusion flame surrounding coal particles during devolatilization in the presence of oxygen.

Soot particles formed from coal contain nitrogen, since the tar from coal also contains nitrogen. This may be important to describing NO_x formation processes in industrial burners. The release of nitrogen from soot has not been examined in detail.

Preliminary measurements of the optical properties of coal-derived soot have been performed using ex situ FTIR extinction techniques, and indicate that the properties of coal-derived soot vary with coal type and residence time. The optical properties of coal-derived soot also differ from soot obtained from propane.

Only one simple model of radiation from soot in a coal combustion system has been developed, and the radiation properties were combined with a turbulence model using an assumed-shape PDF method. Predictions of this simple model performed with and without the presence of soot indicated relatively little change in the gas temperature due to soot radiation. More complex soot formation and radiation models have been developed for gaseous combustion, and the development of a radiation model for coal-derived soot is underway.

It is recommended that additional experiments be performed to determine the cause for large agglomerate formation in post-flame environments, since the presence of large agglomerates in combustion systems introduces the effects of particle scattering. This greatly complicates the radiation model. Additional experiments to relate the optical properties of coal-derived soot to the chemical properties of the parent coal are desired. A robust model to describe the formation, agglomeration, and oxidation of soot particles in coal combustion has not yet been developed; recent data may make the development of such a model feasible.

REFERENCES

1. Haynes, B. S. and Prado, G. P., Soot and PAH Formation in Coal Combustion. EPA/600/8-90/049, 1980.
2. Mengüç, M. P. and Viskanta, R., *Combustion Sci. Technol.*, 1987, **51**, 51.
3. Mengüç, M. P. and Viskanta, R., *Combustion Sci. Technol.*, 1988, **60**, 97.
4. Ahluwalia, R. K. and Im, K. H., *J. Inst. Energy*, 1994, **67**, 23.
5. Im, K. H. and Ahluwalia, R. K., *Int. J. Heat Mass Transfer*, 1993, **36**, 293–302.
6. Ma, J., Soot formation and secondary reactions during coal pyrolysis. Ph.D. thesis, Chemical Engineering Department, Brigham Young University, 1996.
7. Chen, J. C., Castagnoli, C. and Niksa, S., *Energy Fuels*, 1992, **6**, 264–271.
8. Serio, M. A., Hamblen, D. G., Markham, J. R. and Solomon, P. R., *Energy Fuels*, 1987, **1**, 138–152.
9. Nenniger, R. D., Howard, J. B. and Sarofim, A. F., *Sooting Potential of Coals, International Conference on Coal Science*, Pittsburgh, 1983, p. 521.
10. Nenniger, R. D., Aerosols produced from coal pyrolysis, Sc.D. thesis, Department of Chemical Engineering, Massachusetts Institute of Technology, 1986.
11. Wornat, M. J., Sarofim, A. F. and Longwell, J. P., *Energy Fuels*, 1987, **1**, 431.
12. Fletcher, T. H., Solum, M. S., Grant, D. M., Critchfield, S. and Pugmire, R. J., *Twenty-Third Symposium (International) on Combustion*, The Combustion Institute, Pittsburgh, 1990.
13. Ma, J., Fletcher, T. H. and Webb, B. W., *Twenty-Sixth Symposium (International) on Combustion*, The Combustion Institute, Pittsburgh, PA, 1996.
14. Freihaut, J. D., Proscia, W. M. and Seery, D. J., *Energy Fuels*, 1989, **3**, 692–703.
15. McLean, W. M., Hardesty, D. R. and Pohl, J. H., *Eighteenth Symposium (International) on Combustion*, The Combustion Institute, Pittsburgh, 1980, 1239 pp.
16. Seeker, W. R., Samuelson, G. S., Heap, M. P. and Trolinger, J. D., *Eighteenth Symposium (International) on Combustion*, The Combustion Institute, Pittsburgh, 1980. 1213 pp.
17. Ma, J., Fletcher, T. H. and Webb, B. W., *Energy Fuels*, 1995, **9**, 802–808.
18. Wornat, M. J., Sarofim, A. F. and Lafleur, A. L., *Twenty-Fourth Symposium (International) on Combustion*, The Combustion Institute, Pittsburgh, 1992, pp. 955–963.
19. Bruinsma, O. S. L., Geertsma, R. S., Bank, P. and Moulijn, J. A., *Fuel*, 1988, **67**, 327.
20. Bruinsma, O. S. L., Tromp, P. J., Nolting, H. J. and Moulijn, J. A., *Fuel*, 1988, **67**, 334.
21. Doolan, K. R., Mackie, J. C. and Tyler, R. J., *Fuel*, 1987, **66**, 572.
22. Pugmire, R. J., Solum, M. S., Grant, D. M., Critchfield, S. and Fletcher, T. H., *Fuel*, 1991, **70**, 414–423.
23. Freihaut, J. D., Proscia, W. M. and Mackie, J. C., *Combustion Sci. Technol.*, 1993, **93**, 323.
24. Chen, J. C., Effect of secondary reactions on product distribution and nitrogen evolution from rapid coal pyrolysis, Ph.D. thesis, Stanford University, 1991.
25. Chen, J. C. and Niksa, S., *Twenty-Fourth Symposium (International) on Combustion*, The Combustion Institute, Pittsburgh, 1992, 1269 pp.
26. Haynes, B. S., Soot and hydrocarbons in combustion, In: Bartok, W. and Sarofim, A. F. (Eds), *Fossil Fuel Combustion—A Source Book*, John Wiley, New York, 1991, 261 pp.
27. Timothy, L. D., Froelich, D., Sarofim, A. F. and Beer, J. M., *Twenty-First Symposium (International) on Combustion*, The Combustion Institute, 1986, 1141 pp.
28. Musarra, S. P., Fletcher, T. H., Niksa, S. and Dwyer, H. A., *Combustion Sci. Technol.*, 1986, **45**, 289–307.
29. Lau, C. W. and Niksa, S., *Combustion Flame*, 1993, **95**, 1–21.
30. Ma, J., Fletcher, T. H. and Webb, B. W. (Eds), *Effect of Flame Environment on Soot Formation in Coal Combustion*, Elsevier, New York, Vol. 1, 1995, pp. 869–872.
31. Frenklach, M., Clary, D. W., Gardiner, W. C. and Stein, S. E., *Twenty-First Symposium (International) on Combustion*, The Combustion Institute, Pittsburgh, 1986, 1067 pp.
32. Axworthy, A. E., Dayan, V. H. and Martin, G. B., *Fuel*, 1978, **57**, 29.
33. Solomon, P. R. and Colket, M. B., *Fuel*, 1978, **57**, 749.
34. Freihaut, J. D., Zabielski, M. F. and Seery, D. J., *Nineteenth Symposium (International) on Combustion*, The Combustion Institute, Pittsburgh, 1982, 1159 pp.
35. Nelson, P. F., Kelly, M. D. and Wornat, M. J., *Fuel*, 1991, **70**, 402.
36. Kambara, S., Takarada, T., Yamamoto, Y. and Kato, K., *Energy Fuels*, 1993, **7**, 1013.
37. Smith, K. L., Smoot, L. D., Fletcher, T. H. and Pugmire, R. J., *The Structure and Reaction Processes of Coal*, Plenum, New York, 1994.
38. Solomon, P. R. and Fletcher, T. H., *25th Symposium (International) on Combustion*, The Combustion Institute, Pittsburgh, 1994, 463 pp.
39. Houser, T. J., McCarville, M. E. and Biftu, T., *Int. J. Chem. Kinetics*, 1980, **12**, 555.
40. Mackie, J. C., Colket, M. B. and Nelson, P. F., *J. Phys. Chem.*, 1990, **94**, 4099.

41. Mackie, J. C., Colket, M. B., Nelson, P. F. and Esler, M., *Int. J. Chem. Kinetics*, 1991, **23**, 733.
42. Kern, R. D. and Xie, K., *Prog. Energy Combustion Sci.*, 1991, **17**, 191.
43. Wornat, M. J., Sarofim, A. F., Longwell, J. P. and Lafleur, A. L., *Energy Fuels*, 1988, **2**, 775–782.
44. Mengüç, P. C. and Webb, B. W., Radiative heat transfer, In: Smoot, L. D. (Ed.), *Fundamentals of Coal Combustion for Clean and Efficient Use*, Elsevier, New York, 1993, pp. 375–431.
45. Foster, P. J. and Howarth, C. R., *Carbon*, 1968, **6**, 719–729.
46. Habib, Z. G. and Vervisch, P., *Combustion Sci. Technol.*, 1988, **59**, 261–274.
47. Tien, C. L. and Lee, S. C., *Prog. Energy Combustion Sci.*, 1982, **8**, 41–59.
48. Charalampopoulos, T. T. and Felske, J. D., *Combustion Flame*, 1987, **68**, 283–294.
49. Charalampopoulos, T. T. and Chang, H., *Combustion Sci. Technol.*, 1988, **59**, 401–421.
50. Siegel, R. and Howell, J. R., *Thermal Radiation Heat Transfer*, 2nd ed., Hemisphere Publishing, Washington, 1981.
51. Gray, W. A. and Muller, R., *Engineering Calculations in Radiative Heat Transfer*, Pergamon Press, New York, 1974.
52. McCartney, J. T. and Ergun, S., *Fuel*, 1958, **37**, 272–282.
53. Planck, M., *The Theory of Heat Radiation*, Dover Publications, New York, 1959.
54. Brewster, M. Q., *Thermal Radiative Transfer and Properties*, John Wiley, New York, 1992.
55. Avery, D. G., *Proc. Phys. Soc. London*, 1952, **65B**, 425–428.
56. Stagg, B. J. and Charalampopoulos, T. T., *Appl. Optics*, 1991, **30**, 4113–4118.
57. Janzen, J., *J. Colloid Interface Sci.*, 1979, **69**, 436–447.
58. Medallia, A. I. and Richards, L. W., *J. Colloid Interface Sci.*, 1972, **40**, 233–252.
59. Felske, J. D., Charalampopoulos, T. T. and Hura, H. S., *Combustion Sci. Technol.*, 1984, **37**, 263–284.
60. Lee, S. C. and Tien, C. L., *Eighteenth Symposium (International) on Combustion*, The Combustion Institute, Pittsburgh, 1981, pp. 1159–1166.
61. Taft, E. A. and Philipp, H. R., *Phys. Rev.*, 1965, **138**, A197–A202.
62. Senftleben, H. and Benedict, E., *Ann. Phys.*, 1918, **54**, 65–78.
63. Dalzell, W. H. and Sarofim, A. F., *J. Heat Transfer*, 1969, **91**, 100–104.
64. Batten, C. E., *Appl. Optics*, 1985, **24**, 1193–1199.
65. Stagg, B. J. and Charalampopoulos, T. T., *Combustion Flame*, 1993, **94**, 381–396.
66. Tomaselli, V. P., Rivera, R., Edewaard, D. C. and Moller, K. D., *Appl. Optics*, 1981, **20**, 3961–3967.
67. Millikan, R. C., *J. Optical Soc. America*, 1961, **51**, 698–699.
68. Siddall, R. G. and McGrath, I. A., *Ninth Symposium (International) on Combustion*, The Combustion Institute, Pittsburgh, 1963, pp. 102–110.
69. Yasinsky, J. B. and Ergun, S., *Carbon*, 1965, **2**, 355–358.
70. Chippett, S. and Gray, W. A., *Combustion Flame*, 1978, **31**, 149–159.
71. Ku, J. C., Light extinction techniques and related dispersion theories for determining the complex refractive indices of hydrocarbon soots, M.S. thesis, State University of New York at Buffalo, 1982.
72. Erickson, W. D. and Hottel, H. C., *Combustion Flame*, 1964, **8**, 127–132.
73. D'Alessio, A., Di Lorenzo, A., Beretta, F. and Venitozzi, C., *Fourteenth Symposium (International) on Combustion*, The Combustion Institute, Pittsburgh, 1973, pp. 941–953.
74. Buckius, R. O. and Tien, C. L., *Int. J. Heat Mass Transfer*, 1977, **20**, 93–106.
75. Bard, S. and Pagni, P. J., *J. Heat Transfer*, 1981, **103**, 357–362.
76. Powell, E. A. and Zinn, B. T. (Eds), In-Situ *Measurement of the Complex Refractive Index of Combustion Generated Particulates*, Progress in Astronautics and Aeronautics Series, Vol. 92, AIAA, New York, 1983, pp. 238–251.
77. Ben Hamadi, M., Vervisch, P. and Coppalle, A., *Combustion Flame*, 1987, **68**, 57–67.
78. Solomon, P. R., Chien, P. L., Carangelo, R. M., Best, P. E. and Markham, J. R., *Twenty-Second Symposium (International) on Combustion*, The Combustion Institute, Pittsburgh, 1988, pp. 211–221.
79. Sivathanu, Y. R., Gore, J. P., Janssen, J. M. and Senser, D. W., *J. Heat Transfer*, 1993, **115**, 653–658.
80. Koylu, U. O. and Faeth, G. M., *J. Heat Transfer*, 1994, **116**, 152–159.
81. Koylu, U. O. and Faeth, G. M., *J. Heat Transfer*, 1994, **116**, 971–979.
82. Lorentz, H. A., *The Theory of Electrons and Its Application to the Phenomena of Light and Radiant Heat*, 2nd ed., Dover Publications, New York, 1953.
83. Bohren, C. F. and Huffman, D. R., *Absorption and Scattering of Light by Small Particles*, John Wiley, New York, 1983.
84. Rigby, J. R., Webb, B. W. and Fletcher, T. H., *Measurement of the Optical Properties of Coal-derived and Propane-derived Soot in a Flat Flame Reactor*, Western States Section of the Combustion Institute, Tempe, Arizona, 1996.
85. Rigby, J. R., Experimentally determined optical properties and chemical compositions of coal-derived soot, Ph.D. thesis, Brigham Young University, 1996.
86. Sarofim, A. F. and Hottel, H. C., Radiative heat transfer in combustion chambers: influence of alternative fuels, In: *Heat Transfer*, Vol. 6, Hemisphere Publishing Corp., Washington DC, 1978, pp. 199–217.
87. Kent, J. H. and Honnery, D. R., *Combustion Flame*, 1990, **79**, 287–298.
88. Majidi, V., Xu, N. and Saito, K., *Probing Soot Particles Using Laser Based Techniques*, SPIE, Los Angeles, 1994, pp. 146–152.
89. Adams, B. R., Computational evaluation of mechanisms affecting radiation in gas- and coal-fired industrial furnaces, Ph.D. thesis, University of Utah, 1993.
90. Adams, B. R. and Smith, P. J., *Combustion Sci. Technol.*, 1995, **109**, 121–140.
91. Smoot, L. D. and Smith, P. J., *Coal Combustion and Gasification*, Plenum, New York, 1985.
92. Frenklach, M., Development of predictive reaction models of soot formation, Annual Technical Report, Grant No. AFOSR 91-0129, 1991.
93. Leung, K. M., Lindstedt, P. and Jones, W. P., *Combustion Flame*, 1991, **87**, 289–305.
94. Moss, J. B., Stewart, C. D. and Syed, K. J., *Twenty-Second Symposium (International) on Combustion*, The Combustion Institute, Pittsburgh, 1988, pp. 413–423.
95. Moss, J. B., Stewart, C. D. and Young, K. J., *Combustion Flame*, 1995, **4**, 491–500.
96. Kennedy, I. M., Kollmann, W. and Chen, J. Y., *Combustion Flame*, 1990, **81**, 73–85.
97. Honnery, D. R. and Kent, J. H., *Twenty-Fourth Symposium (International) on Combustion*, The Combustion Institute, Pitsburgh, 1992, pp. 1041–1047.
98. Sivathanu, Y. R. and Gore, J. P., *Combustion Flame*, 1994, **97**, 161–172.
99. Coelho, P. J. and Carvalho, M. G., Modeling of Soot Formation in Turbulent Diffusion Flames, Heat Transfer in Fire and Combustion Systems, 1994.

100. Fairweather, M., Jones, W. P. and Lindstedt, R. P., *Combustion Flame*, 1992, **89**, 45–63.
101. Brown, A. L., Modeling soot radiation in coal combustion flames, M.S. thesis, Brigham Young University, 1997.
102. Brown, A. L. and Fletcher, T. H., *Modeling Soot in Coal Combustion Flames*, Western States Section of the Combustion Institute, Los Angeles, CA, 1996.